Cancer Cell
Article

Marginating Dendritic Cells of the Tumor Microenvironment Cross-Present Tumor Antigens and Stably Engage Tumor-Specific T Cells

John J. Engelhardt,[1] Bijan Boldajipour,[1] Peter Beemiller,[1] Priya Pandurangi,[1] Caitlin Sorensen,[1] Zena Werb,[2] Mikala Egeblad,[2,3] and Matthew F. Krummel[1,*]
[1]Department of Pathology
[2]Department of Anatomy
University of California San Francisco, San Francisco, CA 94143, USA
[3]Cold Spring Harbor Laboratory, 1 Bungtown Road, Cold Spring Harbor, NY 11724, USA
*Correspondence: matthew.krummel@ucsf.edu
DOI 10.1016/j.ccr.2012.01.008

SUMMARY

The nature and site of tumor-antigen presentation to immune T cells by bone-marrow-derived cells within the tumor microenvironment remains unresolved. We generated a fluorescent mouse model of spontaneous immunoevasive breast cancer and identified a subset of myeloid cells with significant similarity to dendritic cells and macrophages that constitutively ingest tumor-derived proteins and present processed tumor antigens to reactive T cells. Using intravital live imaging, we determined that infiltrating tumor-specific T cells engage in long-lived interactions with these cells, proximal to the tumor. In vitro, these cells capture cytotoxic T cells in signaling-competent conjugates but do not support full activation or sustain cytolysis. The spatiotemporal dynamics revealed here implicate nonproductive interactions between T cells and antigen-presenting cells on the tumor margin.

INTRODUCTION

Despite the recruitment of tumor-specific $CD8^+$ tumor-infiltrating lymphocytes (TILs) to the tumor microenvironment, the immune response is limited in its ability to clear tumors (Drake et al., 2006). Numerous lines of evidence suggest that tolerance to tumors relies on presentation of peptide antigens on major histocompatibility complex (MHC) molecules on the surface of bone-marrow-derived antigen-presenting cells (APCs), as is the case for other peripheral tissues (Adler et al., 1998; Heath and Carbone, 2001; Kusmartsev et al., 2005; Sotomayor et al., 2001). In recent years, broad classes of cell types derived from the mononuclear phagocyte system (MPS), such as myeloid-derived suppressor cells (MDSCs) and tumor-associated macrophages (TAMs), have been implicated in promoting tumor growth and metastasis while inhibiting a productive immune response by T cells (Gabrilovich and Nagaraj, 2009; Pollard, 2009). TAMs increase metastasis in the PyMT breast cancer model (Lin et al., 2006), partly as a result of T cell skewing toward a Th2 phenotype (DeNardo et al., 2009). Isolated MDSCs bearing the marker Gr-1, in contrast, inhibit T cell activation and suppress the activation of T cells by secondary APCs or other stimuli (Gabrilovich and Nagaraj, 2009; Terabe et al., 2003). There has, however, been no direct identification of the cell type that physically mediates antigen uptake and presentation in the tumor microenvironment.

Dendritic cells (DCs), another cell type derived from the MPS that is very similar to macrophages, are the preeminent APCs for T cells in lymphoid organs and in tissues. DCs in this setting are clearly integral in activating T cells but may also serve to tolerize them (Hawiger et al., 2001). The role of DCs in tumors (TuDC) is less well understood, but their presence is extensively documented. While the elicitation of a potent T cell expansion by DCs is clearly an integral part of a successful immunotherapy and can be augmented by transferring antigen-pulsed DCs to hosts (Mayordomo et al., 1995), DCs in the

Significance

The cells involved in presenting antigens to T cells at the tumor site are not defined. To better study the T cell response to tumors, we developed a fluorescent- and antigen-linked spontaneous model of breast cancer. The primary cells responsible for ingesting tumor antigens and presenting them to T cells are low-motility myeloid cells localized along tumor margins. These cells fail to stimulate T cells and may serve as a barrier to an effective T cell response. This model demonstrates the behavior of tolerized T cells within tumors and provides a target for immunotherapies. Marker analysis demonstrates that the cells presenting antigens to T cells are a large subset of cells implicated in tumor remodeling.

tumor microenvironment may also be an important aspect of immune dysregulation. For example, the presence of specific subsets of DCs, especially CD123$^+$ plasmacytoid DCs (pDCs), are associated with negative prognosis in human patients (Ambe et al., 1989; Treilleux et al., 2004).

Delineating cell types of the MPS purely on surface phenotype has proven difficult because TAMs, MDSCs, and DCs share many common lineage markers. While direct staining of these cells from sections provides information about the populations in aggregate, it is likely that the MPS contributes a variety of cell types to the microenvironment, all of which might be the primary APCs for T cells. Real-time intravital imaging has shed light on key processes during priming in the lymph node, including the priming of T cells on DCs (Miller et al., 2002; Mempel et al., 2004), and holds promise for delineating subsets of APCs that are responsible for interacting with T cells. It has the benefit of complementing phenotypic surface marker data with morphological and behavioral phenotypes. Imaging of ectopic thymomas (EL4s) using labeled T cell receptor (TCR) transgenic cells has revealed long-lived antigen-dependent contacts as well as effective killing between T cells and the tumor cells during tumor rejection (Mrass et al., 2006). However, in those models, there was no possibility to visualize or define the APCs of the microenvironment or to study T cell interaction with such bone-marrow-derived APCs. Furthermore, introduction of tumor-specific T cells in these models leads to tumor regression, unlike the case in typical refractory tumors. Thus, the interactions of T cells and APCs that accompany tumor tolerance have, as yet, remained largely unresolved.

To gain insights into the nature of tumor antigen presentation and the nature of interactions between T cells and APCs in refractory tumors, we have generated a spontaneous tumor model of human breast cancer based on the well-described MMTV-PyMT model (Guy et al., 1992) that incorporates tags for both imaging and for T-cell characterization. This model allows us to track uptake of a coexpressed protein-fluorophore from tumor into the APC compartment. This study effectively exposes a key cell type and its antigen uptake, presentation, and activation capacities, as well as placing these activities spatially within the tumor microenvironment.

RESULTS

Recruitment and Inactivity of Tumor-Specific T Cells in a Spontaneous Model of Breast Cancer

To provide a method for tracking the flow of antigens from tumor to T cell, we generated a spontaneous mouse model for breast cancer in which the initiating oncogene and a neotumor antigen are coexpressed with the stable fluorescent protein mCherry, under a common breast epithelium-specific promoter. For this, we adapted the extensively characterized mouse mammary tumor virus-polyoma middle T (MMTV-PyMT) transgenic cassette (Guy et al., 1992), whose expression gives rise to disease in mice that closely models many aspects of spontaneous luminal breast cancer, including characteristic stages from hyperplasia to adenoma to carcinoma and ultimately to metastatic disease (Lin et al., 2003). We introduced two self-cleaving P2A sequences (de Felipe et al., 2003) downstream of the PyMT cDNA to produce the mCherry and ovalbumin proteins (OVA) (Figure 1A). We included mCherry expression to aid in visualization of transformed cells and to track antigen uptake in the microenvironment. We included OVA to generate germline-encoded self-antigens that were specific to cells expressing the oncogene (“tumor self”) and could be recognized by well-characterized CD8 T cells expressing the OT-I TCR. By coexpressing these genes in a common MMTV-driven transcript, we ensured the coproduction of each protein, in concert with onset of transformation, and yet allowed both mCherry and OVA to be processed independently, thus preventing premature degradation. The expression of these proteins as distinct polypeptides was demonstrated by western blotting (Figure 1B), where each individual protein is detected as a single band at the expected molecular weight. The onset of tumors in this “PyMT ChOVA” line was approximately 20 weeks of age on the C57BL/6 background (Figure S1 available online). The >95% penetrance of tumors and onset at times similar to those of the parental PyMT strain on C57/BL6 background (data not shown) suggested that the inclusion of the mCherry and OVA proteins provided little benefit to the immune system’s ability to recognize or control the tumor.

A sizeable fraction of the tumor antigens that have been isolated from human tumors to date are nonmutated, germline-encoded, tissue-specific proteins that are more dominantly expressed by transformed cells (Finn et al., 1995; Kawakami et al., 1994; van der Bruggen et al., 1991). In these cases, their presumed expression in the thymus apparently leads to negative selection of T cells bearing high-affinity TCRs, and data show a prevalence of cytotoxic T cells (CTLs) with low avidity to these tumor antigens (Gervois et al., 1996), with some notable exceptions identified using tetramers (Lee et al., 1999; Yee et al., 1999). The MMTV promoter used in the PyMT ChOVA model also drove expression in the thymus, as indicated by the negative selection of developing anti-OVA/antitumor OT-I TCR transgenic T cells (Figure 1C). Thus, OVA in this mouse replicates partial central tolerance to tumor antigens.

We next investigated the ability of high-affinity anti-OVA OT-I T cells, introduced into mice already bearing tumors, to respond in situ. Tumor-antigen presentation in PyMT ChOVA lymph nodes was quite robust, as evidenced by proliferation-dependent dilution of the vital dye CFSE specifically in naive tumor-specific T cells (OT-I) in PyMT ChOVA mice, but not in the PyMT mouse strain (Figure 1D). Similarly, introduced GFP-labeled tumor-specific OT-I T cells were present in the tumor and specifically proliferated and accumulated in the lymph node, whereas nonspecific T cells did not expand or significantly populate the tumor (Figure 1E). That the tumor antigen-specific T cells expanded to over 10% of the CD45$^+$ cells and then persisted at high percentages at lymph nodes and tumor for over 30 days (Figure 1F) indicates that the primed cells were not subject to strong deletional tolerance.

Tumor-Specific T Cells Are Incapable of Eliminating PyMT ChOVA Tumors

Tumor-reactive naive T cells are efficiently activated in the secondary lymphoid organs of PyMT ChOVA mice. However, naive high-avidity T cells had only a slight effect in slowing tumor growth and were unable to eliminate tumors when transferred to tumor-bearing hosts (Figures 2A and 2B). These results are

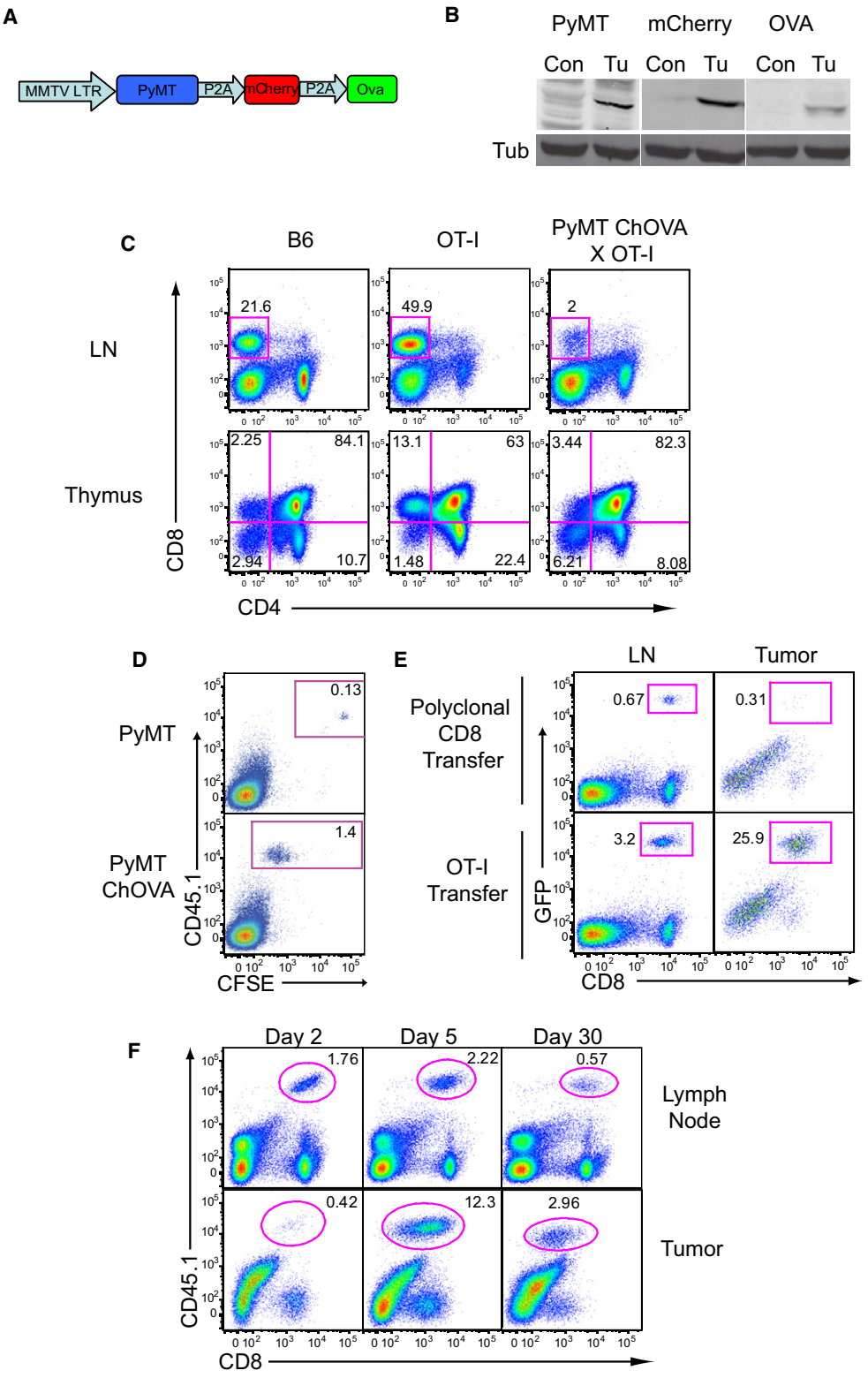

Figure 1. Recruitment and Ineffectiveness of Tumor-Specific T Cells in a Spontaneous Model of Breast Cancer

(A) Schematic of PyMT ChOVA transgenic construct.

(B) Western blots displaying the expression of PyMT, mCherry, and Ova from tumor cells and control T cells in PyMT ChOVA mice.

(C) Thymic negative selection of high-affinity TCRs in the PyMTChOVA spontaneous breast cancer model. Lymph nodes and thymii from wild-type B6, OT-I, or PyMT ChOVA x OT-I mice were analyzed by flow cytometry for CD4 and CD8 expression.

consistent with adoptive transfer of tumor-specific T cells in another spontaneous mouse model, TRAMP, in which lymph node CTL activation fails to be sufficient to induce rejection (Anderson et al., 2007). Notably, in our model, whereas tumor-specific T cells primed for 5 days in the lymph node of tumor-bearing mice demonstrated excellent cytolytic function against antigen-bearing targets, CTL found in the tumor at that time were effectively nonlytic (Figure 2C). That the latter were derived from the former is suggested by the earlier kinetics of accumulation and CFSE dilution in the lymph node relative to the tumor (Figure 1F; data not shown). Overall, this result is similar to human cancers such as melanoma in which tumor-antigen-specific Melan-A/MART-1 tetramer staining demonstrates expanded levels of tumor-specific cells in TILs relative to peripheral sites, coupled with the same profound failure to reject the tumor (Lee et al., 1999; Romero et al., 1998).

We thus sought to determine the in vivo behavior of T cells in our model. To this end, we turned to intravital imaging (Egeblad et al., 2008), adoptively transferring naive GFP-labeled OT-I T cells, allowing them to activate and traffic to tumors and subsequently imaging their interactions in the tumor. We observed significant accumulations of T cells, often in multicellular clusters and at distinct foci along the tumor borders (Figure 2D; Movie S1). As motility appeared much slower near the tumor, we defined a cutoff at 5 μm and considered cells within this radius "proximal," whereas those further away are considered "distal." In tumor-distal regions, T cells were largely motile, moving at 6 μm/min (Figure 2E), a speed only slightly slower than those reported for unrestricted movements in lymph nodes (Miller et al., 2002). However, in the proximal regions, where clusters formed on the tumor margins, speeds were largely reduced to an average of 3 μm/min, with many cells much slower. Radial tracking plots of randomly selected cells supported the theory that most of these cells were in fact swarming or jittering in the proximal clustered regions (Figure 2F), whereas distally located cells quickly diverged from the origin. We did not observe any evidence for destruction of tumor cells by OVA-specific (OT-I) T cells in these tumors, such as single-step loss of mCherry fluorescence in cell-sized voxel regions, consistent with tumor measurements that had previously shown that T cells had little effect on tumor growth.

Phenotypic Characterization of Tumor Antigen Cross-Presenting Dendritic Cells

In engineering the PyMT ChOVA model to coexpress mCherry, we exploited this protein's apparent resistance to degradation to allow us to track antigens that are taken up from tumor cells for presentation by neighboring cells. By flow cytometry, we detected a population of mCherry$^+$/CD45$^+$ cells of hematopoietic origin in single-cell suspensions of PyMT ChOVA but not original PyMT tumors (Figure 3A). A majority of CD45$^+$ cells positive for mCherry above background also expressed high levels of CD11c, an integrin enriched in the dendritic cell lineage. To demonstrate that the mCherry in these cells derived from ingestion of the protein, as opposed to production, we generated bone marrow chimeras in which nontransgenic CD45.1$^+$ bone marrow introduced into PyMT ChOVA mice resulted in mCherry fluorescence in CD11c$^+$ cells of the adopted (transgene-negative) lineage (Figure 3B). We observed mCherry fluorescence as puncta in isolated cells consistent with phagosomes (data not shown) but were unable to detect significant levels of mCherry transcripts in these cells (data not shown), consistent with uptake.

Analysis of CD11c versus Gr-1 staining in the CD45$^+$ mCherry^{hi} cells demonstrated that approximately 3/4 of the mCherry^{hi} cells expressed CD11c and less than 5% of them expressed Gr-1, a marker closely associated with MDSC (Figure 3C). We performed a similar analysis of CD11c and Gr-1 from the entire CD45$^+$ gate (Figure 3D) to characterize the infiltrate in aggregate and thereby defined four populations: CD11c$^+$Gr-1$^-$ (CD11c$^+$), CD11c$^-$ Gr-1$^+$ (Gr-1$^+$), double-positive (CD11c$^+$, Gr-1$^+$), and double-negative (DN). Staining for additional surface proteins showed that none of these subsets expressed CD123, a marker for pDCs; CD135, a marker for bone marrow progenitors; or CD115, the CSF-1R. CD11c$^+$ subsets coexpressed moderate CD11b, whereas Gr-1$^+$ cells expressed distinctly high levels (Figure 3E). The CD11c$^+$ populations also expressed high levels of F4/80 and MHC II. The F4/80 expression together with the CD11b positivity would also qualify this subset as a TAM (Ojalvo et al., 2009). The CD11c$^+$ population also had taken up significantly more of the tumor-derived mCherry than the Gr-1$^+$ or DN populations, although we note that this is bimodal, suggesting the population is not homogeneous in this respect (Figure 3E). The higher levels of both MHC II and mCherry suggests that the CD11c$^+$ cells are most likely to be effective antigen-presenting cells for incoming effector T cells. We also note that they are considerably more abundant within the tumor relative to the other three populations. On an absolute scale, the DP populations were most homogeneously mCherry positive but represented less than 1% of the total isolate. Less than 1% of CD11c$^+$ cells expressed the pDC markers CD123 (Figure 3E) and B220 (data not shown). The best correlation with mCherry positivity was the marker F4/80 (data not shown).

As we were interested in these cells as putative APCs, we next compared the entire lineage of CD11c-positive cells from tumors to splenic DCs and to in-vitro-matured, bone-marrow-derived DCs (BMDCs). CD11c levels were just slightly lower on tumor APCs as compared to BMDCs or splenic DCs (Figure 3F, left panel). When CD11c$^+$ TuDC cells were analyzed, we observed roughly similar levels of MHCs and costimulatory molecule expression in the tumor-associated cells and splenic DCs,

(D) Flow cytometry of tumor-draining lymph nodes 48 hr after 1 × 10^6 CFSE-labeled CD45.1 OT-I T cells were transferred to either a PyMT tumor-bearing mouse or a PyMT ChOVA tumor-bearing mouse.
(E) A total of 5 × 10^6 OT-I-UbGFP T cells or polyclonal Ub-GFP CD8 T cells were transferred to PyMT ChOVA tumor-bearing mice. Five days posttransfer, tumor-draining lymph nodes and tumors were removed and analyzed by flow cytometry. Plots from tumor were previously gated for CD45$^+$ leukocytes.
(F) Tumor-bearing PyMT ChOVA mice received 1 × 10^6 CD45.1 OT-I cells intravenously and were sacrificed at the specified day posttransfer. Tumor-draining lymph nodes and tumor were removed and analyzed by flow cytometry. Plots from tumor were previously gated for CD45$^+$ leukocytes.
See also Figure S1.

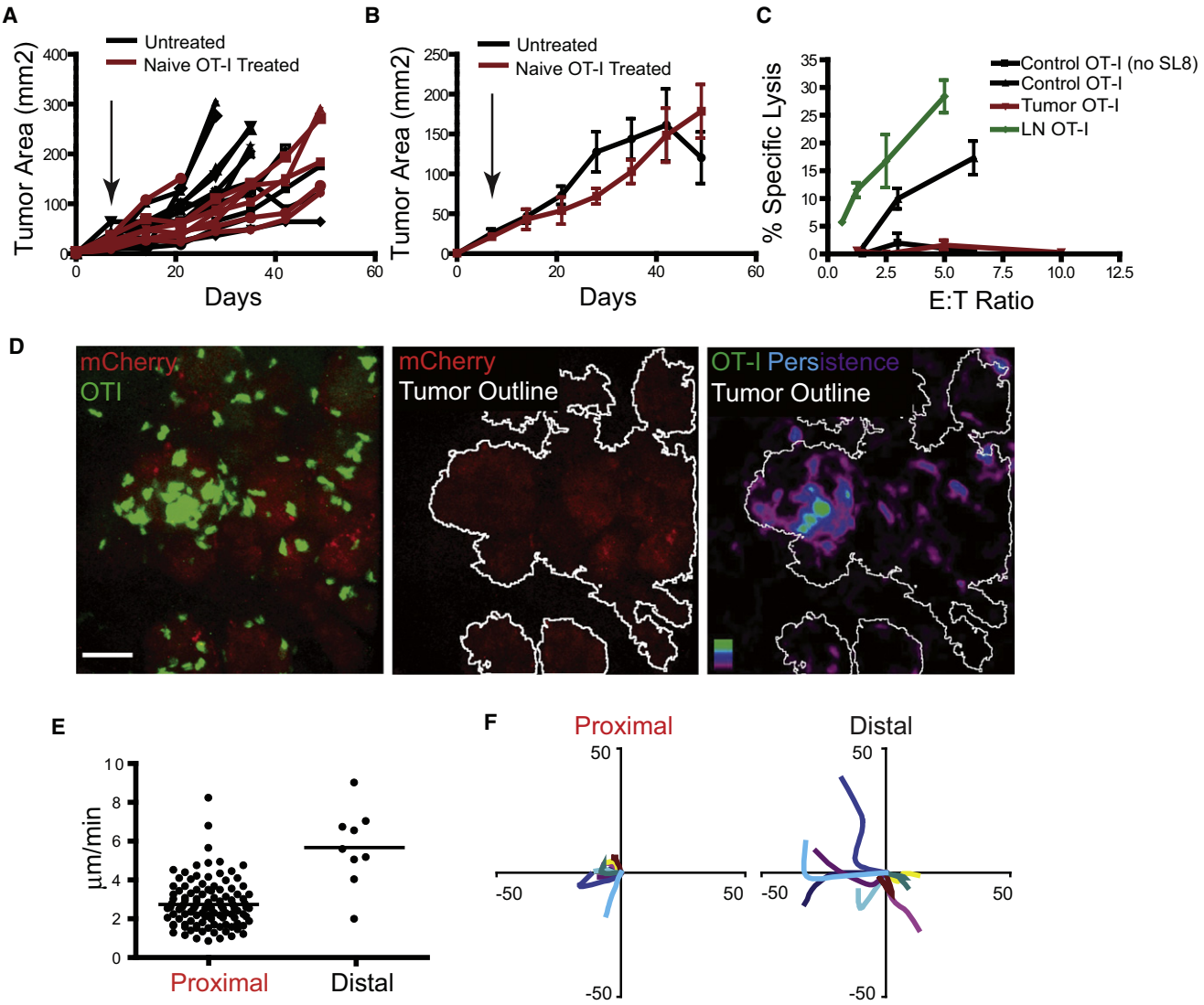

Figure 2. Tumor-Specific T Cells Are Defective in Their Ability to Eliminate PyMT ChOVA Tumors

(A) Tumor burden in individual PyMT ChOVA mice after adoptive transfer of 5 × 10^6 naive OT-I cells (red lines, n = 7) or untreated controls (black lines, n = 12). Arrow indicates date of adoptive transfer.

(B) Average combined tumor burden in PyMT ChOVA mice after adoptive transfer of 5 × 10^6 naive OT-I cells (red line: mean (M) ± SEM, N = 7) or untreated controls (black line: M ± SEM, N = 12).

(C) Cytotoxic activity of OT-I T cells isolated from the lymph nodes (LNs; green) or tumor (red) of PyMTChOva mice 5 days after adoptive transfer, compared to in-vitro-activated control OT-I T cells (black line with triangles) or control OT-I lysis of unpulsed EL4s (black line with squares). A total of 10^4 EL-4 cells (±100 ng/ml SL8 peptide pulse) were used as targets. All lines: M ± SEM, N = 3.

(D) Spinning disc confocal live imaging of OT-I GFP T cells 5 days after adoptive transfer into PyMT ChOVA mice. Representative image of T cell localization at the site of a mCherry fluorescent tumor (left), image displaying tumor area outlined using a threshold mask (middle), and time-average image of T cell persistence at the tumor site with tumors outlined (right). Scale bar, 50 µm.

(E) Average velocity of individual T cell tracks of cells located proximal (within 5 µm) or distal to the tumor.

(F) Representative displacement tracks from T cells located either proximal (within 5 µm) or distal to the tumor border.

See also Movie S1.

suggesting that they would be similarly capable of presenting antigen to naive T cells (Figure 3F). Although many $CD11c^+$ cells at the tumor site were $mCherry^+$, there was still significant heterogeneity within the $CD11c^+$ population for the amount of mCherry that had been ingested. This could reflect that not all cells are in a position to effectively take up the antigen or that the cells degrade the protein over time.

Live Imaging of Tumor Dendritic Cell Behavior

Given the presence of the CD11c protein on the majority of the $mCherry^{hi}$ cells of interest, we interbred PyMT ChOVA mice with mice that express yellow fluorescent protein (YFP) under the control of the CD11c promoter (Lindquist et al., 2004), permitting us to visualize the location and behavior of these APCs directly through real-time intravital live imaging of exposed

tumor masses. Using the same 5 μm proximity cutoffs as in Figure 2, we characterized tumor-proximal CD11c$^+$ cells that were closely juxtaposed with the tumor and had very low motility compared to distal cells (Figures 4A–4C and 4H; Movies S2 and S3). The proximal CD11c-YFP$^+$ cells of the tumors also had the highest level of mCherry fluorescence (Figures 4D, 4E, and 4G; Movie S3). The observation of the behavior of these cells in vivo supported our previous observation that CD11c$^+$ cells ingested tumor antigens and eliminated the possibility that the mCherry fluorescence that we observe by flow cytometry is simply an artifact of in vitro digestion of the tumor. Flow cytometry of tumor from PyMT ChOVA x CD11c YFP mice also demonstrated that CD11c-YFP$^+$ cells from the tumor had taken up mCherry to an extent similar to that in cells stained with antibodies against CD11c supporting the finding that the transgene is generally faithful to the native protein (Figure 4F). Proximal CD11c-YFP$^+$ cells contained significant amounts of mCherry signal in their cytoplasm, often in puncta suggestive of endocytic vesicles, while distal CD11c-YFP$^+$ cells did not contain these structures(Figure 4G). Despite not moving their cell bodies along the tumor margin, these proximal cells dynamically extended and retracted dendrites, which is suggestive of ongoing sampling of the environment (Figure 4H; Movie S3). Morphological data complement phenotypic markers in supporting an assignment of CD11c$^+$ cells from the tumor as DCs, although it is important to remember that the lineages are highly plastic as previously discussed, and these cells may equally be called TAMs on the basis of flow cytometry.

Changes in Myeloid Cell Populations during Tumor Development

Having identified CD11c$^+$ cells as important in ingesting tumor antigens, we sought to characterize whether they were a consistent feature of the tumor across multiple stages. An advantage of the PyMT model is that tumors of distinct developmental stages exist in the same mouse. We identified mice with large carcinomas (area > 100 mm^2) and adenomas (barely palpable tumors < 9 mm^2) at different mammary glands (Figure 5A) and dissociated these tumors for analysis by flow cytometry. After gating on the CD45$^+$ leukocytic infiltrate, we again analyzed the levels of the common myeloid markers, Gr-1, CD11c, CD11b, and F4/80 (Figure 5B). We found that the numbers of cells positive for Gr-1 were significantly higher in carcinomas than adenomas, while CD11c and F4/80 were only modestly increased (Figure 5C). Together, these data suggest that the CD11c$^+$ population is a consistent component of tumors across multiple stages and not restricted to early or late tumors.

Tumor DCs Interact with Tumor-Specific T Cells In Vitro and In Vivo

Armed with the knowledge that this population of CD11c$^+$ cells ingest tumor antigens specifically along the tumor margin, we noted that this location would also ideally place them in a position to interact with the swarming/arrested antigen-specific T cells that we had visualized earlier. To test whether this was the case, we modified our cell-labeling approach to allow direct assessment of interactions between T cells and CD11c$^+$. For this, we transferred OT-I cells derived from mice interbred with the CD2RFP strain, which expresses the RFP protein at a very high level in T cells. We thereby could coimage reactive T cells and the proximal CD11c$^+$ DC in a PyMT ChOVA x CD11c-YFP mouse. In this setting, the mCherry expression of the tumor was considerably less than the RFP-expressing T cells, allowing the latter to be viewed distinctly. We observed both clusters and individual T cells interacting for prolonged periods with tumor-marginal DCs (Figure 6A; Movie S4). We also observed interactions of multiple T cells and DCs that were stable (white arrows) and conjugates of a single T cell with a single DC that formed (blue arrow) or dissipated (yellow arrow) over time.

Analysis of larger fields, using color coding that differentiates lone T cells and DCs from those that are interacting, visually demonstrated that interactions between T cells and DCs were less frequent and more transient in the distal region of the tumor as compared to the proximal region (Figure 6B; Movie S5). Quantification of T cell behaviors over multiple sites demonstrated that the majority of those in clusters, as observed in Figure 6A, were attached to a tumor-proximal DC. Additionally, when individual contacts between T cells and DCs were scored, a large fraction persisted in contact with one another for more than 5 min, with some persisting beyond the 30 min of our standard imaging session. Many of the T cells in the dense clusters persisted there for at least the 30 min periods of our observation. Additionally, when we analyzed whether individual T cells had interacted with a DC during the course of our 30 min imaging session, we found that, by 30 min, 96% (147/153) of T cells had interacted with DCs (defined as contacting DCs), while at the start of acquisition, 56% (85/153) were in contact with DCs. This evidence supports the theory that tumor-proximal T cells are preferentially localized together with the mCherry^{hi} CD11c$^+$ cells in this local environment and that they are effectively engaged in both prolonged and ongoing interactions.

We thus sought to test specifically whether these APCs were more likely to form stable interactions with tumor-specific T cells compared to the OVA$^+$ tumor cells themselves. As it was not possible to distinguish all cell types simultaneously during intravital imaging, we turned to an in vitro system to study T cell coupling frequencies with specific cells of the tumor microenvironment. We prepared single-cell suspensions of all cells from a PyMT ChOVA tumor and allowed the collections of tumor and stromal cells to form couples with a significant excess of in-vitro-activated OT-I T cells and then stained for surface markers to delineate the tumor-derived populations that had interacted. Using CD45$^+$ and MHC II$^+$ as a strategy to highlight all potential APCs with tumor, we demonstrated that T cells preferentially coupled with bone-marrow-derived APCs by this definition compared to tumor cells, even though the latter vastly outnumber them (Figures 6C and 6D). Strikingly, T-cell-engaged APCs had higher levels of mCherry fluorescence than those that failed to couple, suggesting that the T cells differentially couple to the mCherry^{hi} cells (Figure 6E), corresponding to the high frequency of T cell arrest on those proximal mCherry^{hi} cells in vivo (Figure 6B). We applied the same technique to determine if CD11c$^+$ or GR-1$^+$ cells were more likely to interact with OT-I T cells and found that CD11c$^+$ cells were significantly better at forming couples with T cells (Figures 6F and 6G). These results corroborate the observations made during intravital imaging and confirm that T cells preferentially interact with CD11c$^+$ cells when given the opportunity to choose their partner.

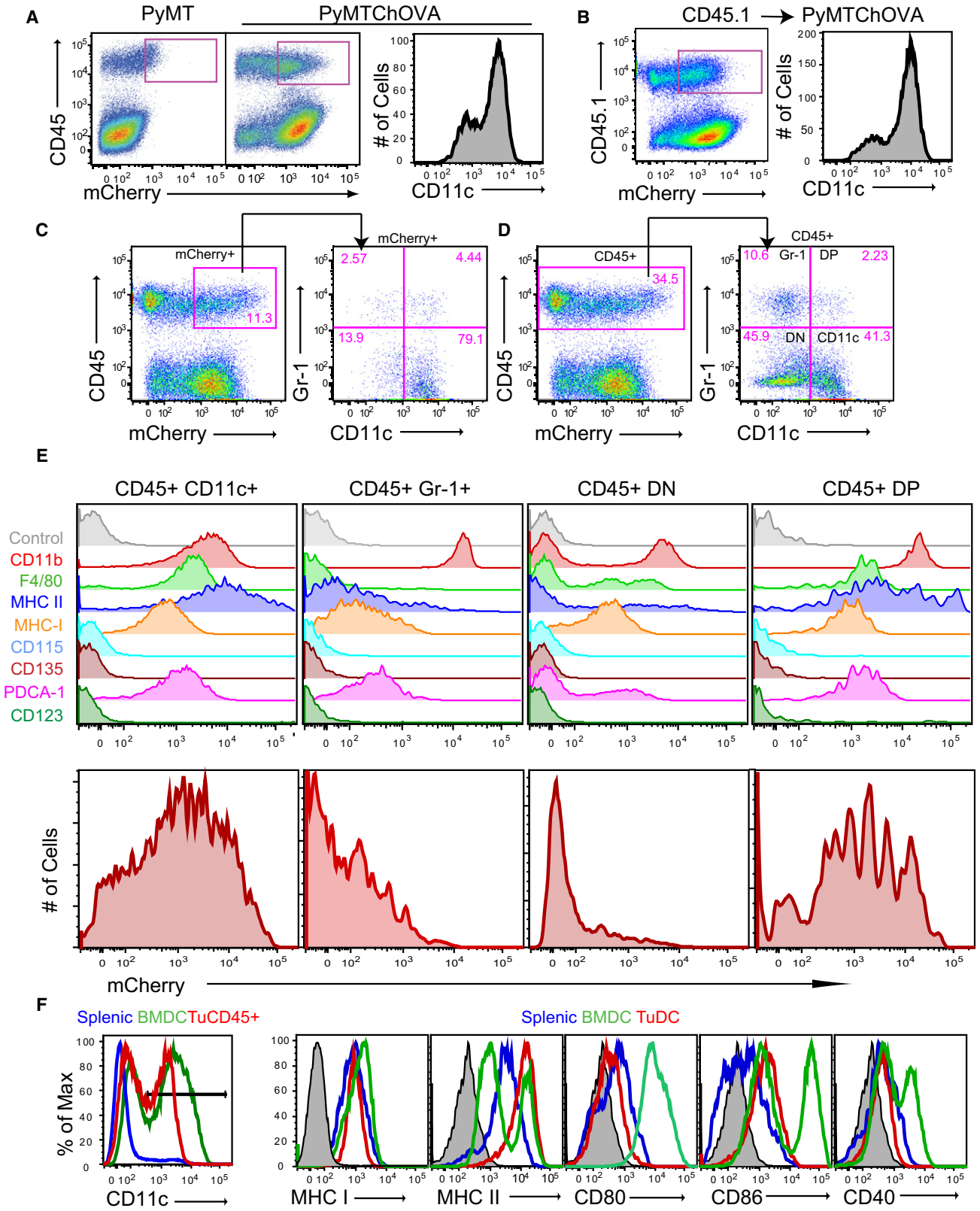

Figure 3. Phenotypic Characterization of Tumor-Antigen Cross-Presenting DCs

(A) Flow cytometry of CD45 expression versus mCherry levels from digested tumor from PyMT (left) or PyMT ChOVA (middle) mice. CD11c levels of gated CD45$^+$ mCherry$^+$ cells (right) from a previous dot plot.

Finally, we investigated the status of TCR levels and the ability to bind pMHC since overall downregulation of the complex is associated with recent signaling (Valitutti et al., 1995) but absence of pMHC binding with presence of the α/β complex has been previously associated with tumor tolerance (Nagaraj et al., 2007). We thus tested the ability of both lymph-node- and tumor-infiltrating T cells to bind to OVA-labeled Kb pentamers 5 days after adoptive transfer into tumor-bearing hosts. We found that both lymph node and tumor OT-I cells both showed decreased levels of pentamer binding in comparison to OT-I cells that were stimulated and then rested for 6 days in vitro, with tumor OT-I showing the lowest level of staining (Figure S2). We similarly determined by staining for the Vβ5 of the OTI TCR that this was decreased in a similar hierarchy in these cells compared to blasted/rested OT-I (Figure S2). We interpret these data as being consistent with ongoing TCR engagement at both lymph node and tumor, leading to downregulation of the entire TCR complex, but not a specific alteration of TCR binding capabilities (e.g., Nagaraj et al., 2007).

Tumor DCs Activate Naive but Not Previously Activated OT-I T Cells

Since activated T cells preferentially interact with the $CD11c^+$ cell populations both in vitro and in vivo, we sought to define the ability of these $CD11c^+$ cells to interact with and stimulate T cells in vitro. Given their cell surface similarity to splenic DC and their mCherry positive phenotype, we were not surprised to find that a total $CD11c^+$/MHC II^+ population, freshly isolated from tumors and without added antigen (TuDCs), stimulated the proliferation of naive OVA-specific (OT-I) T cells in vitro (Figure 7A) at lower but still significantly above background levels compared to BMDCs that had been pulsed with exogenous peptides. This finding established that the TuDCs process and display antigens in peptide-MHC complexes and are capable of stimulating naive T cells, a feature sometimes associated with mature myeloid populations such as mature DCs. However, when assayed for the ability to support proliferation of established CTLs, the tumor-derived antigen-bearing DCs proved unexpectedly incapable of driving cell division. This deficit was true across a wide range of concentrations of DCs and even when exogenous peptides were added to the TuDCs (Figure 7B), suggesting that the block was profound.

However, live imaging of CTLs, labeled with the calcium dye FURA-2 and interacting with TuDCs, demonstrated that proximal activation occurred in CTL and that peptide-MHC triggering of TCRs at the site of these interactions was not defective (Figure 7C; Movies S6 and S7). Both the percentage of cells that generated calcium transients during interaction (Figure 7D) and the magnitude of calcium curves generated by a panel of cells (Figure 7E) were similar between TuDCs and the stimulatory BMDC population pulsed with exogenous peptides. These results are consistent with peptide-MHC expression on these cells but suggest that TuDCs apparently might bear inhibitory ligands that function distal to synapse formation and TCR signaling and inhibit productive responses. We also tested the ability of TuDCs to induce upregulation of CD69 on previously activated T cells and found that CD69 is upregulated by T cells stimulated by both BMDCs pulsed with peptide and TuDCs (Figure S3). These data support the conclusion that TuDCs are indeed antigen positive and are also able to initiate early events of TCR signaling. We screened a large number of candidate molecules and pathways and eliminated the canonical T cell inhibitory pathways that are suggested to function in MDSCs, M2 macrophages, and other APCs, including both surface receptors and soluble factors (Figure S3). That none of these restored proliferation suggests an unknown mechanism of T cell inhibition.

Given the ability of these TuDCs to support antigen-dependent coupling with CTLs in vitro and in vivo, we sought to determine the downstream effects of these signaling interactions. We therefore tested the ability of CTLs encountering the TuDCs to maintain CTL function, a key deficit in T cells that had homed to the tumor (Figure 2). Comparisons of cytolysis by T cells cultured with TuDCs showed that this interaction does not sustain cytolytic function, similar to T cells cultured alone or T cells stimulated with BMDCs without peptide. In contrast, T cells cultured with BMDC pulsed with peptides or T cells cultured alone or with TuDCs in the presence of interleukin-2 (IL-2) did maintain cytolytic acitivity (Figure 7F).

As we were unable to restore proliferation effectively by blocking established inhibitory pathways in these assays, we also sought to reverse the phenotype by modulating the DC. Maturing the TuDCs by adding either imiquimod or CpG to the stimulation reaction strikingly relicensed them to stimulate CTLs to further divide (Figure 7G). These two agents are agonists for APC-expressed toll-like receptors (TLRs) 7 and 9, respectively, and neither agent had significant effects on the T cells (data not shown). As a control, cells were treated without effect by applying lipopolysaccharide (LPS), an agonist to TLR4, which is poorly expressed by TuDCs (data not shown). Supplementing the stimulation reaction with exogenous cytokines, whether IL-2, IL-12, or IL-15, also was able to rescue the proliferative defect (Figure 7H). Together, our data suggest a specific stimulatory defect of TuDCs in their interactions with CTL, separate from antigen processing and presentation.

Given the ability of these TuDCs to support antigen-dependent interactions with CTLs, we finally sought to determine whether TuDCs suppress CTLs from responding to other antigen-presenting cells. While, in some experiments, inhibition was profound, it was inconsistent over 13 experiments with an

(B) Flow cytometry of CD45.1 expression versus mCherry levels from bone marrow chimera made by adoption of CD45.1 bone marrow cells into an irradiated PyMT ChOVA mouse.
(C) CD45 expression versus mCherry levels from digested tumor from PyMT ChOVA mouse, gated $CD45^+$ $mCherry^{hi}$ cells were propagated to subsequent dot plot and analyzed for their expression of CD11c and Gr-1.
(D) CD45 expression versus mCherry levels from digested tumor from PyMT ChOVA mouse, gated $CD45^+$ cells were propagated to subsequent dot plot and analyzed for their expression of CD11c and Gr-1.
(E) Gated and labeled populations from (3D) were analyzed for their expression of the listed cell surface markers or for their mCherry fluorescence level.
(F) $CD11c^+$ cells from the spleens of B6 mice, BMDC cultures, or the tumor of PyMT ChOVA mice. Gate in left histogram propagated to subsequent histograms.

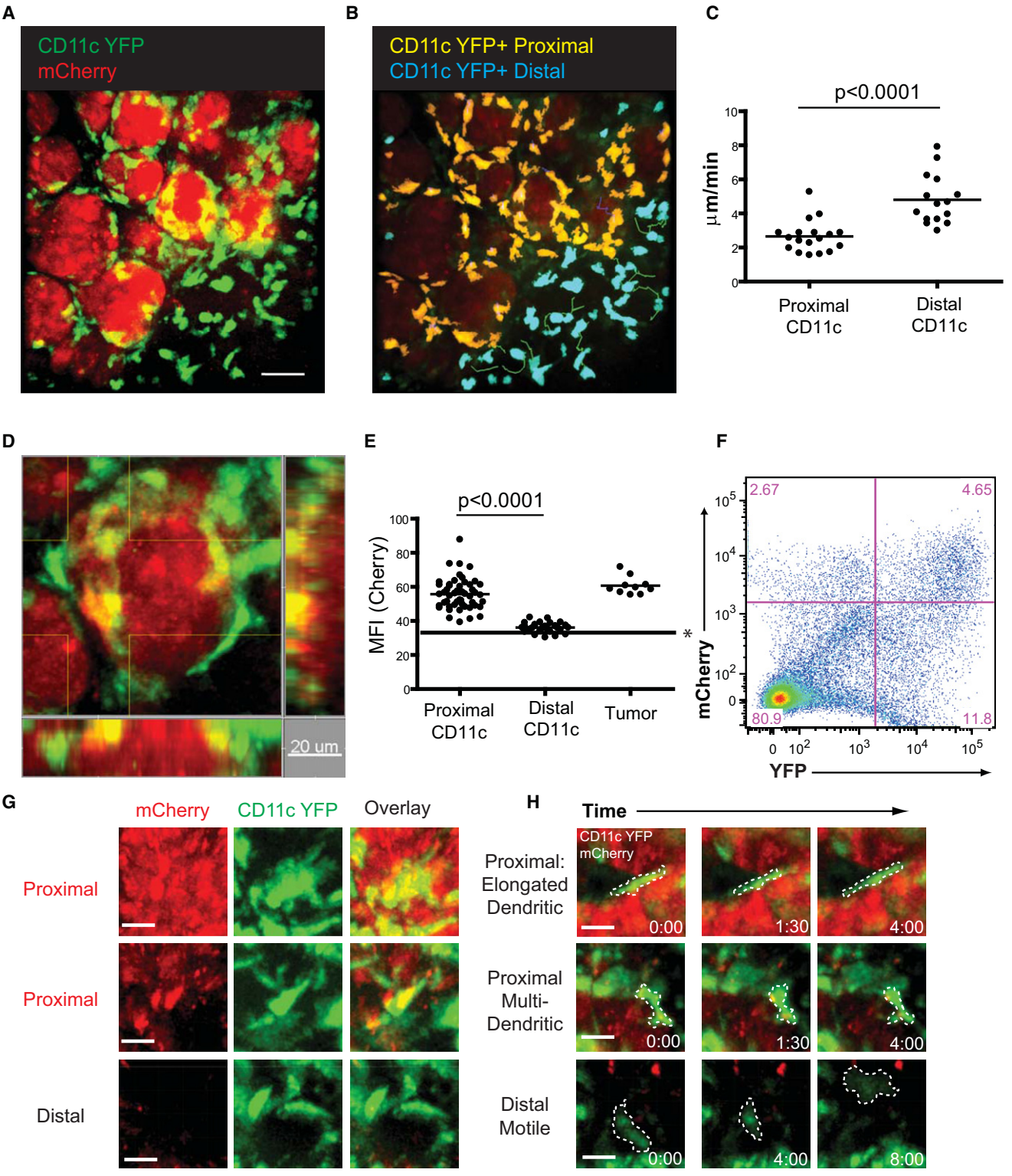

Figure 4. Live Imaging of Tumor-DC Behavior

(A) Representative still image acquired by intravital spinning disc confocal microscopy of mCherry$^+$ CD11c YFP$^+$ DCs in PyMT ChOVA x CD11c YFP mice. Scale bar, 10 μm.

(B) DCs are color coded based on their proximity to the tumor border. Proximal DCs (within 5 μm) are coded yellow, and distal DCs (>5 μm from tumor border) are coded blue. Color-coded DCs with representative tracks of their movement during imaging.

(C) Average velocity of individual CD11c YFP$^+$ cells located proximal or distal to the tumor border.

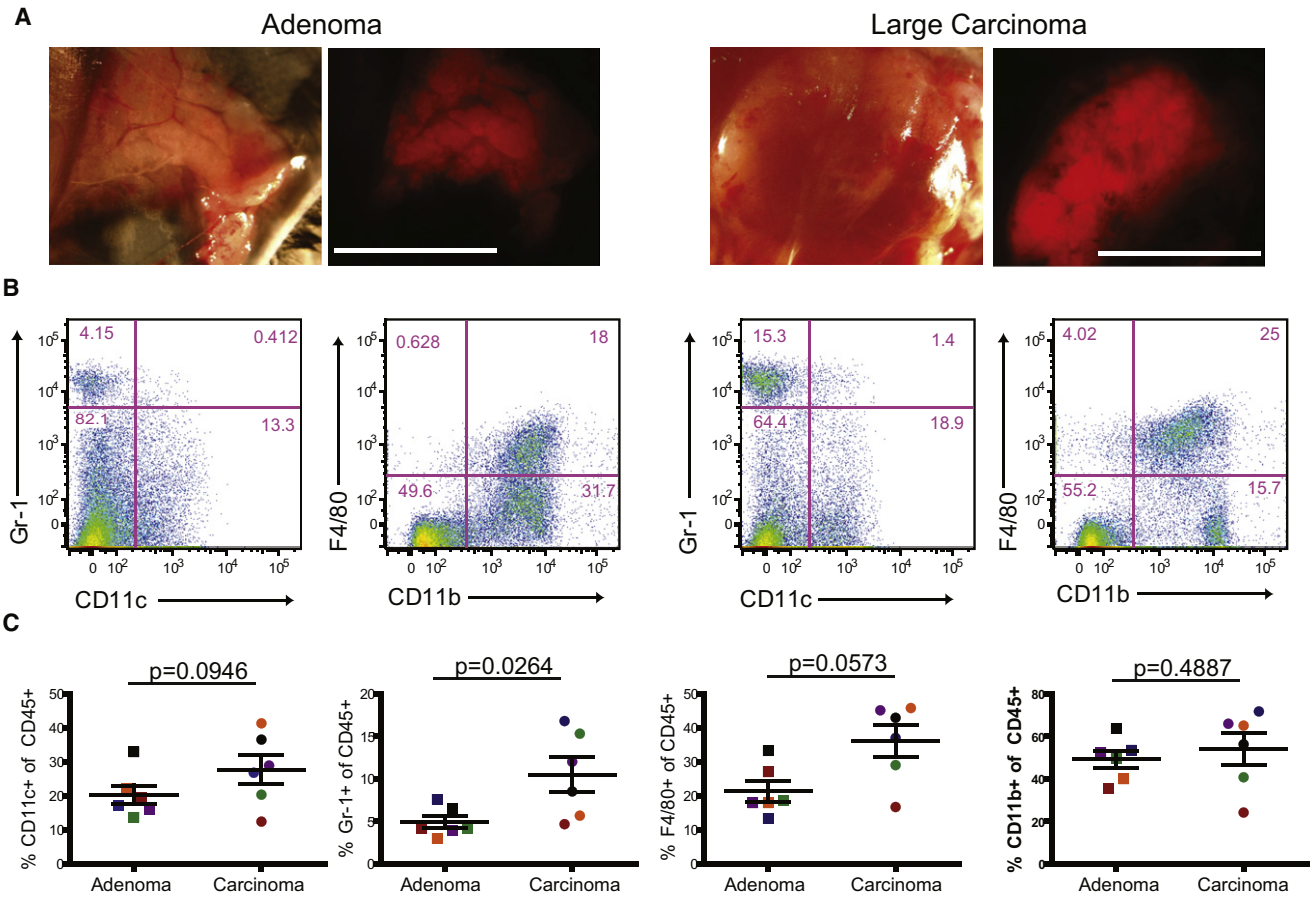

Figure 5. Alteration of Leukocytic Infiltrate with Tumor Development

(A) Transmitted and mCherry-fluorescent images of tumors from PyMT ChOVA mouse taken on a dissecting scope. Scale bar, 1 cm.

(B) Cells from either an adenoma or a late carcinoma tumor were dissociated and analyzed by flow cytometry. $CD45^+$ cells were analyzed for the cell surface markers CD11c, Gr-1, CD11b, and F4/80.

(C) Plots depict percent positive for specified cell surface markers out total $CD45^+$ cells from tumors at different stages. Each data point represents one tumor, and matched colors indicate tumors were from the same mouse.

average of just 30% inhibition (Figure S3). Since we do not yet understand the mechanisms utilized, any dominant suppression, if present, may also be sensitive to culture conditions or may be reversible (e.g., see Figure 7G). Alternatively, given the paucity of other effective APCs in the tumor microenvironment, tolerance may result purely from ineffective or defective repriming.

DISCUSSION

Delineating APCs in Tumors

Using a spontaneous mouse model of breast cancer, we have identified a population of myeloid cells that is optimized for ingesting and presenting tumor antigens to CD8 T cells and, thus, is a clear and relevant APC of the tumor microenvironment. This formal identification is an important finding since many cells are likely capable of antigen presentation in vitro when pulsed appropriately with peptides, yet no previous study has been able to unequivocally define the cells that interact with tumor-specific T cells within tumors. The direct demonstration of their presence at the site of T cell arrest along the margin suggest that they fill this roll in vivo as well as in vitro.

Ojalvo et al. recently described TAMs as c-fmsGFP$^+$ F4/80$^+$ and dextran$^+$ (Ojalvo et al., 2009); by this definition, the mCherry$^+$ cells that we describe here could also be classified as TAMs, as they are CD11b$^+$ and F4/80$^+$ and their mCherry positivity largely substitutes for dextran$^+$ as a marker of phagocytic ability (J.J.E.

(D) Representative still image acquired by intravital spinning disc confocal microscopy of mCherry$^+$ CD11c YFP$^+$ DCs in PyMT ChOVA x CD11c YFP mice.

(E) Mean fluorescent intensity of CD11c YFP$^+$ cells located proximal or distal to the tumor border, and tumor masses. Line indicated with an asterisk represents background fluorescence of image.

(F) Flow cytometry analysis of CD11c-YFP x PyMT ChOVA mouse displaying CD11c YFP$^+$ mCherry$^+$ DCs.

(G) Representative YFP, mCherry, and overlay still images of DCs either proximal or distal to the tumor. Scale bar, 10 μm.

(H) Representative still images of YFP$^+$ cells displaying either dendritic-like or motile cell behaviors. Cell outlines are marked in dashed lines. Scale bar, 10 μm. See also Movies S2 and S3.

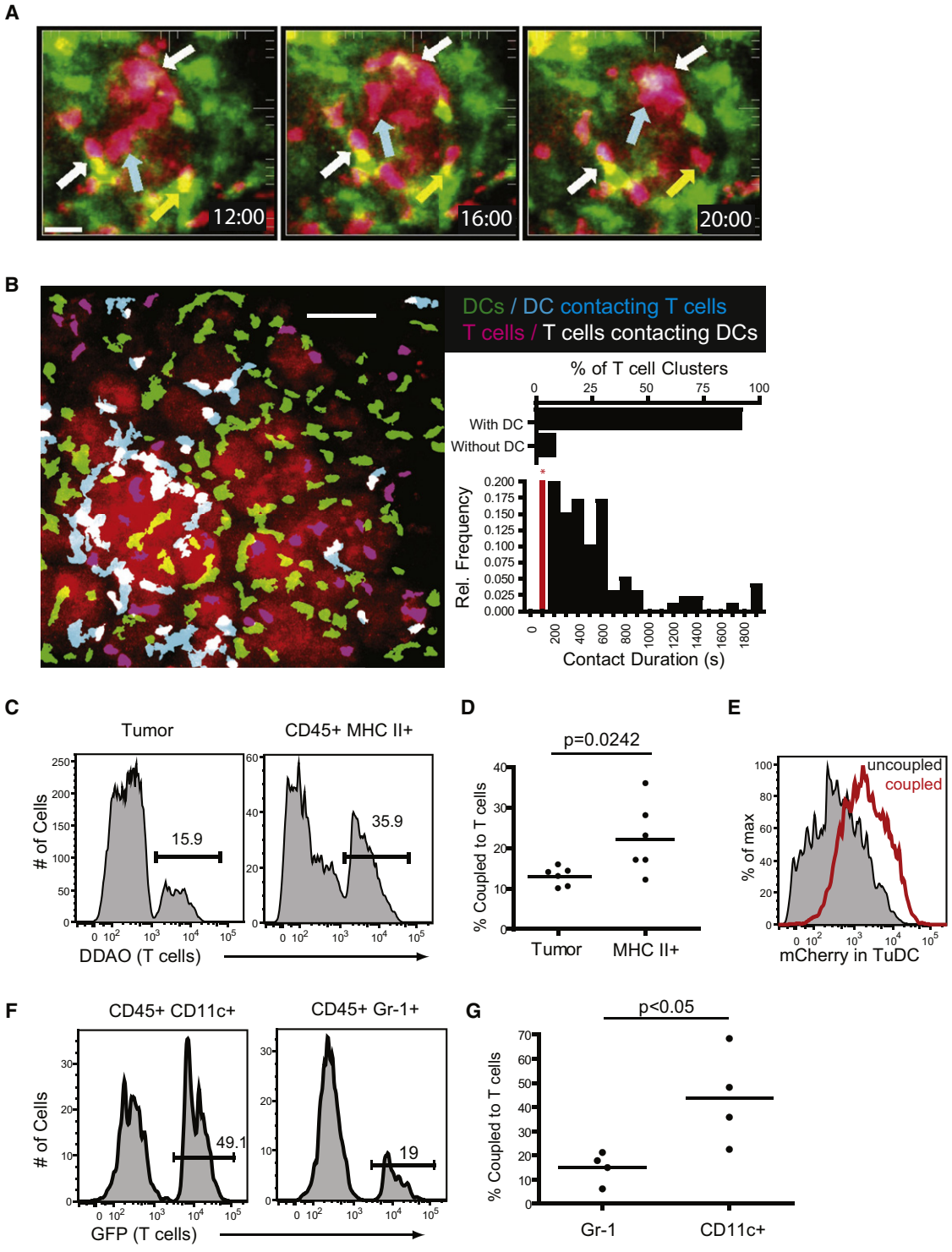

Figure 6. Tumor DCs Interact with Tumor-Specific T Cells In Vitro and In Vivo

(A) Spinning disc confocal imaging of CD2RFP OT-I T cells 5 days after adoptive transfer to PyMT ChOVA x CD11c-YFP mice. A representative image sequence of CD2RFP T cells (red) interacting with CD11c-YFP (green) DCs at the tumor site; white arrows indicate T cells interacting with DCs throughout the time lapse, yellow arrows indicate a T cell leaving an interaction with a DC, and blue arrows indicate a T cell moving to a DC. Scale bar, 30 μm.

(B) Representative image displaying T cells (red) and DCs (green) at the tumor site. Blue cells indicate DCs contacting T cells (defined by overlapping red and green fluorescence), and white cells indicate T cells contacting DCs. Scale bar, 50 μm. Inset/top: Graph of the number of T cell clusters (defined as stable groups of greater than 2 T cells) that occur with DCs present or without DCs present. Inset/bottom: Relative frequency of contact duration between OT-I T cells and TuDCs. Pairs with contact durations lower than 200 s were not considered.

and M.F.K., unpublished data). Although we do not find significant expression of CD115, the protein product of the c-fms GFP reporter, the TuDC population we describe otherwise can be considered a substantial subset of TAMs as well, and the nomenclature discrepancy in the literature may ultimately resolve these on the basis of data such as ours. The plasticity and overlap of cell surface markers makes the study and classification of these cells difficult, but we suggest classifying these cells as dendritic cells for immunological purposes, based on their cell surface marker expression and in vivo morphology and behavior. This apparent equivalency in the literature is then intriguing, as some of the same cells that are implicated in tolerizing T cells are also those implicated in remodeling and angiogenesis (Schoppmann et al., 2002; Qian and Pollard, 2010).

We have excluded tumor APCs from the MDSC population because of their lack of expression of the defining marker for this population, Gr-1, and furthermore because the CD11c$^+$ cells do not function in analogous manner; namely, defective proliferation is not restored with iNOS and/or Arginase inhibition (Figure S2) (Gabrilovich and Nagaraj, 2009). Although we identify CD11c$^+$ cells to be a distinct subset of cells from the entire lineage of the MPS, we acknowledge that some of these cells have previously been described by others as TAMs (DeNardo et al., 2009) or MDSCs or that some of our cells may share phenotypic or functional characteristics of these populations. However, the method that we have used clearly highlights this population of cells on the basis of location, morphology, phagocytosis, and their unique interactions with infiltrating T cells. It is also important to note that transient TCR-triggering interactions might occur with other APCs at sites besides the proximal region, and we cannot rule out interactions between T cells and the few CD11c$^-$ mCherry$^+$ APCs. We have demonstrated in the lymph nodes that even transient interactions can trigger TCR clustering and/or internalization (Friedman et al., 2010). Although, with our in vitro coupling experiments and in vivo behavioral studies, we established that CD11c$^+$ TuDC are the predominant partners for T cells, this by no means excludes other members of the MPS from ever acting on T cells via antigen receptors.

Despite the robust mCherry signal in tumor CD45+ cells, we were unable to detect mCherry$^+$ DCs in the tumor-draining lymph nodes (data not shown). It thus remains unknown how and by which cells antigen is being presented to lymph node T cells. DCs from the tumor site may be trafficking to lymph nodes but degrading the mCherry protein, or soluble tumor antigens may travel through the lymph directly.

The Behavior of Tumor-Specific T Cells in Refractory Tumors

In addition to identifying the tumor antigen cross-presenting DCs at the tumor site, we were also able to study the behavior of tumor antigen-specific T cells in a spontaneous and progressive model that is refractory to large numbers of infiltrating tumor-specific T cells. While activation and proliferation of naive tumor-specific T cells was robust in the lymph node, these T cells were shown to be defective at lysis of targets after exposure to the tumor microenvironment. This lack of cytolytic ability correlated with a lack of therapeutic benefit to adoptive transfer of T cells. This inactivity is similar to what is seen in human vaccination trials where large numbers of tumor-specific T cells can be elicited without eliminating tumors (Gattinoni et al., 2006; Rosenberg et al., 2005), suggesting a later defect, as we are observing in this model. The ability of exogenous γc cytokines to restore proliferation of T cells is also consistent with higher levels of efficacy of adoptive cell therapy when combined with IL-2 or IL-15 administration (Gattinoni et al., 2005; Overwijk et al., 2003; Epardaud et al., 2008).

Intravital imaging in our model revealed strong long-lasting interactions between tumor-specific T cells and DCs at the tumor site. The importance of interactions between T cells and DCs at the effector site of an immune response is an emerging field of study; in the case of viral infections, the stimulation of memory or effector cells by DCs at peripheral sites is thought to be important for effective viral immunity (Wakim et al., 2008). The behavior of these ineffective tumor-specific T cells is different from the behavior of tumor-rejecting T cells described in previous studies of ectopic tumor models (Mrass et al., 2006). While that study highlighted the activity of a strongly productive T cell response to a tumor, our study represents the activity occurring in a tumor setting that is more representative of naturally occurring human disease, where TILs are not effective in controlling tumor growth. It remains to be determined why T cells preferentially interact with TuDCs as compared to other cells of the tumor, and it is intriguing to conjecture that a specific chemokine-driven interaction may also contribute both to cell positioning within the tumor and, perhaps, to the limited stimulation capacity.

Tolerance Induction through T-APC Interactions within the Tumor

The concept that a BMDC serves to tolerize T cells that interact with them as cognate APCs is not unprecedented. Tolerance in the lymph node occurs when antigens are directed to DEC205$^+$ DCs in the lymph nodes in the absence of additional stimuli (Hawiger et al., 2001). Adler et al. broadly described the requirement for MHC-matched BMDCs in the tolerance to a tissue-restricted antigen (Adler et al., 1998), and induction of tolerance to an A20 lymphoma required matched bone marrow cells and not the tumors themselves (Sotomayor et al., 2001).

Based on our in vitro studies, we propose that the interaction between T cells and DCs may in fact inhibit the ongoing T cell response or, alternatively, may simply fail to effectively restimulate T cells to control the tumor while diverting them into such "sterile" interactions. After isolation of tumor DCs, we found that they were capable of activating naive T cells to proliferate but not in-vitro-generated activated T cells. A recent report

(C) Histogram displaying the percentage of tumor cells (left) or MHC II$^+$ cells (right) from PyMT ChOVA tumors that form couples with DDAO-labeled T cells.
(D) Results from six separate coupling assays plotted as percentage of tumor or MHC II$^+$ cells coupled to T cells. Bar represents mean.
(E) mCherry fluorescence of CD45$^+$ MHC class II$^+$ cells that were not coupled to T cells (shaded histogram) or were coupled to T cells (red histogram).
(F) Histogram displaying the percentage of mCherry$^+$ CD11c$^+$ or CD45$^+$ Gr-1$^+$ cells that form couples with OT-I GFP T cells.
(G) Results from four separate coupling assays plotted as percentage of CD11c or GR-1$^+$ cells coupled to T cells. Bar represents mean.
See also Figure S2 and Movies S4 and S5.

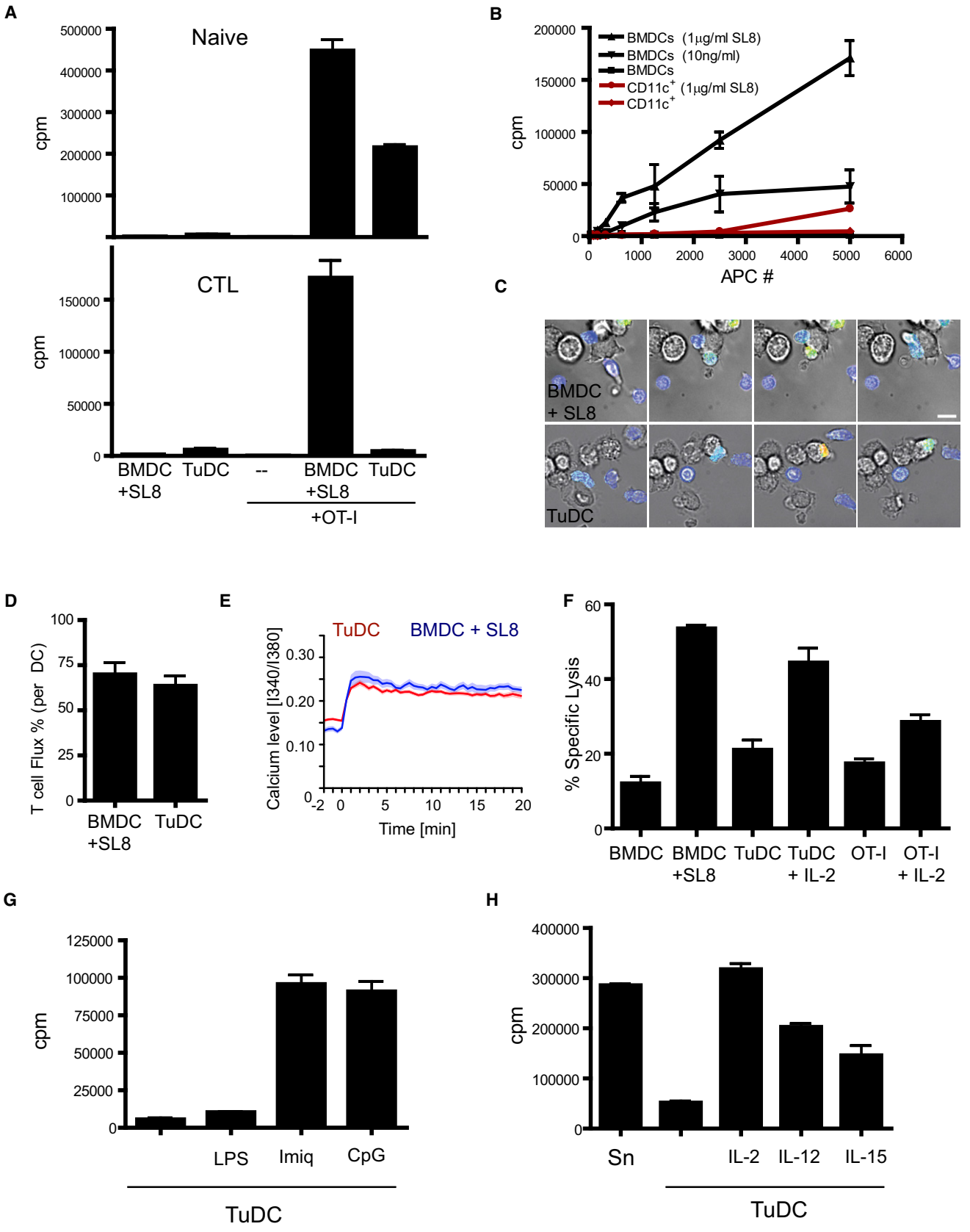
A
Naive
CTL
cpm
BMDC +SL8
TuDC
--
BMDC +SL8
TuDC
+OT-I
B
BMDCs (1μg/ml SL8)
BMDCs (10ng/ml)
BMDCs
CD11c+ (1μg/ml SL8)
CD11c+
APC #
C
BMDC + SL8
TuDC
D
T cell Flux % (per DC)
E
TuDC
BMDC + SL8
Calcium level [I340/I380]
Time [min]
F
% Specific Lysis
BMDC
BMDC +SL8
TuDC
TuDC + IL-2
OT-I
OT-I + IL-2
G
LPS
Imiq
CpG
TuDC
H
Sn
IL-2
IL-12
IL-15
TuDC

describing TuDCs isolated from the NeuT model of mammary carcinoma demonstrated an inhibitory phenotype for these cells when exogenously pulsed with peptides and used to stimulate naive CD8 T cells (Norian et al., 2009). While similar to our findings, the differences—that our cells are able to stimulate naive CD8s while theirs are not and that their inhibition was mediated by arginine metabolism—suggest that the mechanism of inhibition is distinct.

The defect in T cell restimulation exhibited by TuDCs could be rescued by treatment of the cultures with the TLR agonists CpG DNA and imiquimod. These data suggest that TuDCs are either specifically lacking a stimulatory signal or are actively giving an inhibitory signal that is distinct from other stimulatory DCs. These data are consistent with a previous study in another spontaneous tumor model, RIP-Tag, where adoptive cell therapy was only effective in conjunction with CpG administration (Garbi et al., 2004) Similarly, topical administration of imiquimod was effective against some established tumors in an ectopic model (Lu et al., 2010), and it is tempting to speculate that this TuDC/CTL axis is being modulated in that case. Topical application of imiquimod to breast tissue was not effective in our hands (data not shown). TuDCs from imiquimod-treated mice or after treatment in vitro had similar levels of MHC II, CD80, and CD86 when compared to untreated TuDCs. Our highest doses of imiquimod sometimes led to tumor hemorrhaging, and so we suspect that a more direct approach toward modifying TuDC function will be necessary.

Additional in vitro data correlate the functionally inactive T cells at the tumor site to DC interactions. T cells cultured with tumor DCs, but not stimulatory BMDCs, are unable to maintain lytic activity against targets, again suggesting that this interaction is deficient in its ability to promote a strong tumor response. Both the intravital imaging detailing interactions between T cells and DCs at the tumor site and in vitro coupling assays indicate that T cells are preferentially drawn to DCs as they enter the tumor microenvironment. Since this interaction fails to promote T cell effector function, it may be a significant impediment to the ongoing tumor response.

Does this represent a new mechanism of T cell tolerance? We have examined a large variety of surface receptor and soluble mediators and find that these do not revert inhibition and allow proliferation. It is interesting that we can demonstrate that proximal signaling, both as assessed by calcium signaling and, indirectly, through the formation of stable T cell and TuDC couples, is intact. Otten and Germain had previously described a state of "split anergy" in CTL clones; T cells retained cytotoxicity but lost proliferation and IL-2 secretion, when these lines engaged partially fixed APCs (Otten and Germain, 1991). The situation in response to TuDCs has interesting parallels, although inverted; the key defect for tumor rejection may in fact be the loss of CTL function.

Implications for Immunotherapy

Current immunotherapies focus on promoting a strong antitumor T cell response by altering the T cells themselves, either by increasing tumor-specific T cell frequency by adoptive cell transfer (Dudley et al., 2002), increasing the reactivity of responding T cells by engineering of high-avidity TCRs specific for tumors (Park et al., 2011), or by eliciting more potent T cells by blockade of inhibitory costimulatory molecules such as CTLA-4 or PD-1. While CTLA-4 blockade, in particular, has shown promise in treating human melanoma, many patients still show no clinical response after treatment (Hodi et al., 2010). The reasons behind this are unknown, but our data suggest that tumor-based APCs may function by a unique mechanism and that combination therapy to boost T cell responses via CTLA-4 blockade in conjunction with treatments that alter TuDC stimulatory capacity may be particularly effective. Our model in many ways represents a best-case scenario for immunotherapy in that we have available a large number of high-avidity, tumor-specific T cells for adoptive therapy. That treatment with this therapy still fails highlights the need to search for other ways to enhance the T cell response within tumors.

EXPERIMENTAL PROCEDURES

Mice and Genotyping

PyMT ChOVA transgenic C57BL/6 founder mice were generated as described in the associated Supplemental Information. All other mice are as described in the Supplemental Information. All mice were maintained in microisolator cages and treated in accordance with National Institutes of Health (NIH) and American Association of Laboratory Animal Care standards, consistent with the animal care and use regulations of the Institutional Animal Care and Use Committee of the University of California, San Francisco (UCSF).

Cell Tracking and Imaging Analysis

We visualized and analyzed data using Imaris 5.7.2 and 7.0 Software (Bitplane). Individual cells were identified and tracked by Imaris, and cell speed

Figure 7. Tumor DCs Activate Naive but Not Previously Activated OT-I T Cells

(A) Proliferation of either naive (upper) or previously activated (lower) OT-I T cells activated with either sorted TuDCs (50,000) or BMDCs (5,000) pulsed with 100 ng/ml SL8 peptide. N = 3 M ± SEM.

(B) Proliferation of previously activated OT-I T cells cultured with varying numbers of TuDCs or BMDCs pulsed with the specified amount of SL8 peptide. N = 3 M ± SEM.

(C) Live imaging of previously activated and Fura-2 labeled OT-I T cells interacting with BMDCs pulsed with 100 ng/ml SL8 peptide or with TuDCs. Brightfield images are overlaid with a pseudocolor image of the ratiometric Fura-2 fluorescence values, with low intracellular calcium levels represented in blue and high intracellular calcium represented in red. Scale bar, 10 μm.

(D) Frequency of cell contacts with SL8 peptide-pulsed BMDCs or TuDCs that lead to calcium transients in previously activated OT-I T cells. N = 3 M ± SEM.

(E) Intracellular calcium levels of previously activated OT-I T cells contacting BMDCs pulsed with 100 ng/ml SL8 peptide or TuDC. Mean values with standard errors are shown.

(F). Cytolytic activity of in-vitro-activated T cells after overnight culture with BMDCs, TuDCs, or BMDCs pulsed with 100 ng/ml SL8 peptide. N = 3 M ± SEM.

(G) Proliferation of OT-I T cells cultured with TuDCs alone or TuDCs with the TLR ligands, LPS (1 μg/ml), imiquimod (2.5 μg/ml), or CpG (10 μg/ml). N = 3 M ± SEM.

(H) Proliferation of OT-I T cells cultured with either control splenocytes pulsed with 100 ng/ml SL8 peptide or TuDCs alone or in the presence of IL-2 (3 U/ml), IL-12 (10 ng/ml), or IL-15(10 ng/ml). N = 3 M ± SEM.

See also Figure S3 and Movies S6 and S7.

and displacement were calculated from tracks. Mean fluorescence intensity of mCherry in CD11c YFP DCs was calculated using iso-surfaces of masked DCs from MATLAB segmentation. Contact duration was determined by calculated track duration of masked T cell and DC couples that were tracked using Imaris. T cell clusters for analysis of presence of DCs in couples were defined as clusters of T cells containing more than two T cells. The presence of DCs contacting these clusters was determined by visual inspection. Statistical analysis of speeds, stopping times, mean fluorescence intensity, and interaction times was conducted with Prism 4.0 (GraphPad Software), using an unpaired t test and a two-tailed 95% confidence interval.

Statistical Analysis

Statistical analyses were performed with GraphPad Prism. Unless specifically noted, all data are representative of >3 separate experiments. Error bars represent SEM, were calculated using Prism, and are derived from triplicate experimental conditions. Specific statistical tests used were paired and unpaired t tests, and all p values < 0.05 were considered statistically significant.

SUPPLEMENTAL INFORMATION

Supplemental Information includes three figures, Supplemental Experimental Procedures, and seven movies and can be found with this article online at doi:10.1016/j.ccr.2012.01.008.

ACKNOWLEDGMENTS

We thank A. Ma, L. Lanier, and N. Matsumoto for advice and the generous sharing of materials. We also thank Nigel Killeen and the UCSF Transgenic Core for assistance in the production of transgenic mice and Cliff MacArthur and Shu-Wei Jiang for assistance with cell sorting. This work was supported by NIH Grants R01CA134622, R01CA129523, U01CA141451, and by the Cancer Research Institute. B.B. was supported by an EMBO fellowship, and J.J.E. was supported by NIH Training Grant CA108462. We thank Mark Anderson, Alexis Madrid, and Emily Thornton for critical reading of the manuscript. We thank Lisa Coussens, David Denardo, Brian Ruffell, and Vicki Plaks for helpful discussions.

Received: July 29, 2011
Revised: November 18, 2011
Accepted: January 13, 2012
Published: March 19, 2012

REFERENCES

Adler, A.J., Marsh, D.W., Yochum, G.S., Guzzo, J.L., Nigam, A., Nelson, W.G., and Pardoll, D.M. (1998). CD4+ T cell tolerance to parenchymal self-antigens requires presentation by bone marrow-derived antigen-presenting cells. J. Exp. Med. *187*, 1555–1564.

Ambe, K., Mori, M., and Enjoji, M. (1989). S-100 protein-positive dendritic cells in colorectal adenocarcinomas. Distribution and relation to the clinical prognosis. Cancer *63*, 496–503.

Anderson, M.J., Shafer-Weaver, K., Greenberg, N.M., and Hurwitz, A.A. (2007). Tolerization of tumor-specific T cells despite efficient initial priming in a primary murine model of prostate cancer. J. Immunol. *178*, 1268–1276.

de Felipe, P., Hughes, L.E., Ryan, M.D., and Brown, J.D. (2003). Co-translational, intraribosomal cleavage of polypeptides by the foot-and-mouth disease virus 2A peptide. J. Biol. Chem. *278*, 11441–11448.

DeNardo, D.G., Barreto, J.B., Andreu, P., Vasquez, L., Tawfik, D., Kolhatkar, N., and Coussens, L.M. (2009). CD4(+) T cells regulate pulmonary metastasis of mammary carcinomas by enhancing protumor properties of macrophages. Cancer Cell *16*, 91–102.

Drake, C.G., Jaffee, E., and Pardoll, D.M. (2006). Mechanisms of immune evasion by tumors. Adv. Immunol. *90*, 51–81.

Dudley, M.E., Wunderlich, J.R., Robbins, P.F., Yang, J.C., Hwu, P., Schwartzentruber, D.J., Topalian, S.L., Sherry, R., Restifo, N.P., Hubicki, A.M., et al. (2002). Cancer regression and autoimmunity in patients after clonal repopulation with antitumor lymphocytes. Science *298*, 850–854.

Egeblad, M., Ewald, A.J., Askautrud, H.A., Truitt, M.L., Welm, B.E., Bainbridge, E., Peeters, G., Krummel, M.F., and Werb, Z. (2008). Visualizing stromal cell dynamics in different tumor microenvironments by spinning disk confocal microscopy. Dis. Model Mech. *1*, 155–167.

Epardaud, M., Elpek, K.G., Rubinstein, M.P., Yonekura, A.R., Bellemare-Pelletier, A., Bronson, R., Hamerman, J.A., Goldrath, A.W., and Turley, S.J. (2008). Interleukin-15/interleukin-15R alpha complexes promote destruction of established tumors by reviving tumor-resident CD8+ T cells. Cancer Res. *68*, 2972–2983.

Finn, O.J., Jerome, K.R., Henderson, R.A., Pecher, G., Domenech, N., Magarian-Blander, J., and Barratt-Boyes, S.M. (1995). MUC-1 epithelial tumor mucin-based immunity and cancer vaccines. Immunol. Rev. *145*, 61–89.

Friedman, R.S., Beemiller, P., Sorensen, C.M., Jacobelli, J., and Krummel, M.F. (2010). Real-time analysis of T cell receptors in naive cells in vitro and in vivo reveals flexibility in synapse and signaling dynamics. J. Exp. Med. *207*, 2733–2749.

Gabrilovich, D.I., and Nagaraj, S. (2009). Myeloid-derived suppressor cells as regulators of the immune system. Nat. Rev. Immunol. *9*, 162–174.

Garbi, N., Arnold, B., Gordon, S., Hämmerling, G.J., and Ganss, R. (2004). CpG motifs as proinflammatory factors render autochthonous tumors permissive for infiltration and destruction. J. Immunol. *172*, 5861–5869.

Gattinoni, L., Klebanoff, C.A., Palmer, D.C., Wrzesinski, C., Kerstann, K., Yu, Z., Finkelstein, S.E., Theoret, M.R., Rosenberg, S.A., and Restifo, N.P. (2005). Acquisition of full effector function in vitro paradoxically impairs the in vivo antitumor efficacy of adoptively transferred CD8+ T cells. J. Clin. Invest. *115*, 1616–1626.

Gattinoni, L., Powell, D.J., Jr., Rosenberg, S.A., and Restifo, N.P. (2006). Adoptive immunotherapy for cancer: building on success. Nat. Rev. Immunol. *6*, 383–393.

Gervois, N., Guilloux, Y., Diez, E., and Jotereau, F. (1996). Suboptimal activation of melanoma infiltrating lymphocytes (TIL) due to low avidity of TCR/MHC-tumor peptide interactions. J. Exp. Med. *183*, 2403–2407.

Guy, C.T., Cardiff, R.D., and Muller, W.J. (1992). Induction of mammary tumors by expression of polyomavirus middle T oncogene: a transgenic mouse model for metastatic disease. Mol. Cell. Biol. *12*, 954–961.

Hawiger, D., Inaba, K., Dorsett, Y., Guo, M., Mahnke, K., Rivera, M., Ravetch, J.V., Steinman, R.M., and Nussenzweig, M.C. (2001). Dendritic cells induce peripheral T cell unresponsiveness under steady state conditions in vivo. J. Exp. Med. *194*, 769–779.

Heath, W.R., and Carbone, F.R. (2001). Cross-presentation, dendritic cells, tolerance and immunity. Annu. Rev. Immunol. *19*, 47–64.

Hodi, F.S., O'Day, S.J., McDermott, D.F., Weber, R.W., Sosman, J.A., Haanen, J.B., Gonzalez, R., Robert, C., Schadendorf, D., Hassel, J.C., et al. (2010). Improved survival with ipilimumab in patients with metastatic melanoma. N. Engl. J. Med. *363*, 711–723.

Kawakami, Y., Eliyahu, S., Delgado, C.H., Robbins, P.F., Rivoltini, L., Topalian, S.L., Miki, T., and Rosenberg, S.A. (1994). Cloning of the gene coding for a shared human melanoma antigen recognized by autologous T cells infiltrating into tumor. Proc. Natl. Acad. Sci. USA *91*, 3515–3519.

Kusmartsev, S., Nagaraj, S., and Gabrilovich, D.I. (2005). Tumor-associated CD8+ T cell tolerance induced by bone marrow-derived immature myeloid cells. J. Immunol. *175*, 4583–4592.

Lee, P.P., Yee, C., Savage, P.A., Fong, L., Brockstedt, D., Weber, J.S., Johnson, D., Swetter, S., Thompson, J., Greenberg, P.D., et al. (1999). Characterization of circulating T cells specific for tumor-associated antigens in melanoma patients. Nat. Med. *5*, 677–685.

Lin, E.Y., Jones, J.G., Li, P., Zhu, L., Whitney, K.D., Muller, W.J., and Pollard, J.W. (2003). Progression to malignancy in the polyoma middle T oncoprotein mouse breast cancer model provides a reliable model for human diseases. Am. J. Pathol. *163*, 2113–2126.

Lin, E.Y., Li, J.-F., Gnatovskiy, L., Deng, Y., Zhu, L., Grzesik, D.A., Qian, H., Xue, X.N., and Pollard, J.W. (2006). Macrophages regulate the angiogenic switch in a mouse model of breast cancer. Cancer Res. *66*, 11238–11246.

Lindquist, R.L., Shakhar, G., Dudziak, D., Wardemann, H., Eisenreich, T., Dustin, M.L., and Nussenzweig, M.C. (2004). Visualizing dendritic cell networks in vivo. Nat. Immunol. *5*, 1243–1250.

Lu, H., Wagner, W.M., Gad, E., Yang, Y., Duan, H., Amon, L.M., Van Denend, N., Larson, E.R., Chang, A., Tufvesson, H., and Disis, M.L. (2010). Treatment failure of a TLR-7 agonist occurs due to self-regulation of acute inflammation and can be overcome by IL-10 blockade. J. Immunol. *184*, 5360–5367.

Mayordomo, J.I., Zorina, T., Storkus, W.J., Zitvogel, L., Celluzzi, C., Falo, L.D., Melief, C.J., Ildstad, S.T., Kast, W.M., Deleo, A.B., et al. (1995). Bone marrow-derived dendritic cells pulsed with synthetic tumour peptides elicit protective and therapeutic antitumour immunity. Nat. Med. *1*, 1297–1302.

Mempel, T.R., Henrickson, S.E., and Von Andrian, U.H. (2004). T-cell priming by dendritic cells in lymph nodes occurs in three distinct phases. Nature *427*, 154–159.

Miller, M.J., Wei, S.H., Parker, I., and Cahalan, M.D. (2002). Two-photon imaging of lymphocyte motility and antigen response in intact lymph node. Science *296*, 1869–1873.

Mrass, P., Takano, H., Ng, L.G., Daxini, S., Lasaro, M.O., Iparraguirre, A., Cavanagh, L.L., von Andrian, U.H., Ertl, H.C., Haydon, P.G., and Weninger, W. (2006). Random migration precedes stable target cell interactions of tumor-infiltrating T cells. J. Exp. Med. *203*, 2749–2761.

Nagaraj, S., Gupta, K., Pisarev, V., Kinarsky, L., Sherman, S., Kang, L., Herber, D.L., Schneck, J., and Gabrilovich, D.I. (2007). Altered recognition of antigen is a mechanism of CD8+ T cell tolerance in cancer. Nat. Med. *13*, 828–835.

Norian, L.A., Rodriguez, P.C., O'Mara, L.A., Zabaleta, J., Ochoa, A.C., Cella, M., and Allen, P.M. (2009). Tumor-infiltrating regulatory dendritic cells inhibit CD8+ T cell function via L-arginine metabolism. Cancer Res. *69*, 3086–3094.

Ojalvo, L.S., King, W., Cox, D., and Pollard, J.W. (2009). High-density gene expression analysis of tumor-associated macrophages from mouse mammary tumors. Am. J. Pathol. *174*, 1048–1064.

Otten, G.R., and Germain, R.N. (1991). Split anergy in a CD8+ T cell: receptor-dependent cytolysis in the absence of interleukin-2 production. Science *251*, 1228–1231.

Overwijk, W.W., Theoret, M.R., Finkelstein, S.E., Surman, D.R., de Jong, L.A., Vyth-Dreese, F.A., Dellemijn, T.A., Antony, P.A., Spiess, P.J., Palmer, D.C., et al. (2003). Tumor regression and autoimmunity after reversal of a functionally tolerant state of self-reactive CD8+ T cells. J. Exp. Med. *198*, 569–580.

Park, T.S., Rosenberg, S.A., and Morgan, R.A. (2011). Treating cancer with genetically engineered T cells. Trends Biotechnol. *29*, 1–8.

Pollard, J.W. (2009). Trophic macrophages in development and disease. Nat. Rev. Immunol. *9*, 259–270.

Qian, B.-Z., and Pollard, J.W. (2010). Macrophage diversity enhances tumor progression and metastasis. Cell *141*, 39–51.

Romero, P., Dunbar, P.R., Valmori, D., Pittet, M., Ogg, G.S., Rimoldi, D., Chen, J.L., Liénard, D., Cerottini, J.C., and Cerundolo, V. (1998). Ex vivo staining of metastatic lymph nodes by class I major histocompatibility complex tetramers reveals high numbers of antigen-experienced tumor-specific cytolytic T lymphocytes. J. Exp. Med. *188*, 1641–1650.

Rosenberg, S.A., Sherry, R.M., Morton, K.E., Scharfman, W.J., Yang, J.C., Topalian, S.L., Royal, R.E., Kammula, U., Restifo, N.P., Hughes, M.S., et al. (2005). Tumor progression can occur despite the induction of very high levels of self/tumor antigen-specific CD8+ T cells in patients with melanoma. J. Immunol. *175*, 6169–6176.

Schoppmann, S.F., Birner, P., Stöckl, J., Kalt, R., Ullrich, R., Caucig, C., Kriehuber, E., Nagy, K., Alitalo, K., and Kerjaschki, D. (2002). Tumor-associated macrophages express lymphatic endothelial growth factors and are related to peritumoral lymphangiogenesis. Am. J. Pathol. *161*, 947–956.

Sotomayor, E.M., Borrello, I., Rattis, F.M., Cuenca, A.G., Abrams, J., Staveley-O'Carroll, K., and Levitsky, H.I. (2001). Cross-presentation of tumor antigens by bone marrow-derived antigen-presenting cells is the dominant mechanism in the induction of T-cell tolerance during B-cell lymphoma progression. Blood *98*, 1070–1077.

Terabe, M., Matsui, S., Park, J.M., Mamura, M., Noben-Trauth, N., Donaldson, D.D., Chen, W., Wahl, S.M., Ledbetter, S., Pratt, B., et al. (2003). Transforming growth factor-beta production and myeloid cells are an effector mechanism through which CD1d-restricted T cells block cytotoxic T lymphocyte-mediated tumor immunosurveillance: abrogation prevents tumor recurrence. J. Exp. Med. *198*, 1741–1752.

Treilleux, I., Blay, J.Y., Bendriss-Vermare, N., Ray-Coquard, I., Bachelot, T., Guastalla, J.P., Bremond, A., Goddard, S., Pin, J.J., Barthelemy-Dubois, C., and Lebecque, S. (2004). Dendritic cell infiltration and prognosis of early stage breast cancer. Clin. Cancer Res. *10*, 7466–7474.

Valitutti, S., Müller, S., Cella, M., Padovan, E., and Lanzavecchia, A. (1995). Serial triggering of many T-cell receptors by a few peptide-MHC complexes. Nature *375*, 148–151.

van der Bruggen, P., Traversari, C., Chomez, P., Lurquin, C., De Plaen, E., Van den Eynde, B., Knuth, A., and Boon, T. (1991). A gene encoding an antigen recognized by cytolytic T lymphocytes on a human melanoma. Science *254*, 1643–1647.

Wakim, L.M., Waithman, J., van Rooijen, N., Heath, W.R., and Carbone, F.R. (2008). Dendritic cell-induced memory T cell activation in nonlymphoid tissues. Science *319*, 198–202.

Yee, C., Savage, P.A., Lee, P.P., Davis, M.M., and Greenberg, P.D. (1999). Isolation of high avidity melanoma-reactive CTL from heterogeneous populations using peptide-MHC tetramers. J. Immunol. *162*, 2227–2234.